Publication I

J. Särkkä and A. Harju. 2008. Spin dynamics in a double quantum dot: Exact diagonalization study. Physical Review B, volume 77, number 24, 245315, pages 1-6.

Spin dynamics in a double quantum dot: Exact diagonalization study

J. Särkkä and A. Harju
Helsinki Institute of Physics and Department of Engineering Physics, Helsinki University of Technology, P.O. Box 4100, FI-02015 TKK, Finland

(Received 2 April 2008; revised manuscript received 20 May 2008; published 13 June 2008)

We study spin dynamics and singlet-triplet decoherence due to the hyperfine interaction in a parabolic double quantum dot. We use exact diagonalization and perturbation theory for calculating the time evolution of the wave function. The probabilities for the singlet state exhibit damped oscillations and converge toward a value, which depends only on the strength of the hyperfine field and the exchange energy. We derive expressions for the asymptotic singlet probability and its variance using a 2×2 effective Hamiltonian matrix. The asymptotic values and variances for singlet probabilities are in agreement with previous experimental data.

DOI: 10.1103/PhysRevB.77.245315 PACS number(s): 73.21.La, 71.70.Gm, 71.70.Jp, 85.35.Be

I. INTRODUCTION

The progress of nanotechnology has made the construction of a quantum computer a realistic goal. Several alternatives for a quantum bit, the building block of a quantum computer, have been considered. The Loss-DiVincenzo scheme[1] proposing semiconductor quantum dots for qubits has spurred various studies concerning this realization.[2–6] Extensive studies, for example, have been made on a two-electron double quantum dot.[7–13]

The decoherence is always a significant obstacle in quantum computing. In semiconductor quantum dots, decoherence is mainly caused by the hyperfine interaction with 10^5 lattice nuclei with spin 3/2[14–19] and spin-orbit interaction with lattice phonons.[20,21] Decoherence due to the spin-orbit interaction has a timescale from 100 μs to 100 ms,[10,22,23] whereas decoherence of hyperfine interaction has a timescale of 10 ns.[11,13] Hence, as recent experiments show, for times under 10 μs in low temperatures the hyperfine interaction is the most significant decoherence mechanism.[13,24] The dipolar interaction between the nuclei changes the individual nuclear-spin orientations. This interaction is weak, having a time scale of 100 μs for a finite magnetic field.[25] Considering that the spin-diffusion time for nuclei in the vicinity of donors exceeds one second,[26] the nuclear spins may be approximated as frozen in the timescale of hyperfine-induced dephasing. The spin dephasing times may be increased by nuclear polarization and projective measurement resulting in the narrowing of the nuclear-spin distribution.[27–29]

The singlet-triplet decoherence due to the hyperfine interaction was studied theoretically by Coish and Loss.[30] Their model predicts damped oscillations and a saturation value for the singlet probability that depends only on the ratio of the rms hyperfine interaction strength and the exchange energy. Laird *et al.*[24] measured the singlet-triplet decoherence of an electron pair in a GaAs double dot. By varying the gate voltage, they modified the exchange energy J and observed changes in the oscillations and saturation of the spin correlator. There have been only a few exact diagonalization studies of hyperfine dephasing, mainly concerning single spin decay[31,32] and a recent study of a two-electron quantum dot.[33]

In this paper, we study the effect of exchange interaction on hyperfine-induced singlet-triplet decoherence in a parabolic double quantum dot. We obtain similar values for the exchange energy as observed in the experiments of Laird *et al.*[24] by adjusting the external voltage properly in the calculations. The eigenstates and eigenvectors of the two-electron Hamiltonian are solved using exact diagonalization. We calculate the time evolution of the singlet probability and compare the results with the experimental results. In the time evolution, we first solve the four lowest eigenstates without hyperfine field. The 4×4 Hamiltonian matrix that includes hyperfine fields is then constructed using exact diagonalization. This method enables the study of various dot geometries and perturbations. We also analyze the dependence of the spin variance on the spin expectation value and derive expressions for the asymptotic singlet probability and its variance using a 2×2 effective Hamiltonian.

II. MODEL AND METHOD

We model the two-electron system with the Hamiltonian,

$$H=\sum_{i=1}^{2}\left[\frac{\left(-i\hbar\nabla_i-\frac{e}{c}\mathbf{A}\right)^2}{2m^*}+V(\mathbf{r}_i,\mathbf{s}_i)\right]+\frac{e^2}{\epsilon r_{12}}. \tag{1}$$

The external potential V consists of two parts,

$$V=V_Z+V_C, \tag{2}$$

where V_Z is the potential caused by the Zeeman interaction,

$$V_Z(\mathbf{r},\mathbf{s})=g^*\mu_B\mathbf{B}(\mathbf{r})\cdot\mathbf{s}, \tag{3}$$

and the Lande factor of GaAs is $g^*=-0.44$. The magnetic field can be divided into a homogeneous external magnetic field $\mathbf{B}_{\text{ext}}$ and an inhomogeneous random hyperfine field $\mathbf{B}_{\text{nuc}}(\mathbf{r})$. The second part in the external potential is the confinement potential V_C, similar to the potential used by Helle *et al.*,[34]

$$V_C(\mathbf{r})=\frac{1}{2}m^*\omega_0^2\left\{\min\left[\sum_{j=1}^{2}(\mathbf{r}-\mathbf{L}_j)^2\right]-2L_Tx\right\}, \tag{4}$$

where $\mathbf{L}_j$ gives the positions of the minima of the confinement potential and the detuning parameter L_T is proportional to the strength of the biased potential due to the external voltage. The confinement potential is illustrated in Fig. 1.

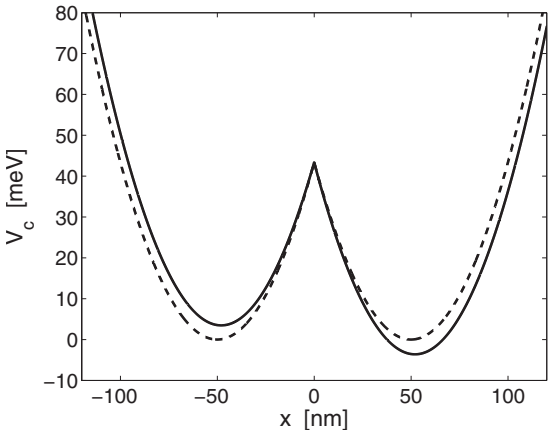

FIG. 1. Confinement potential $V_c(x,0)$ and $L_x=50$ nm for detuning parameters $L_T=0$ nm (dashed) and $L_T=20$ nm (solid).

The cusp in the potential at $x=0$ does not affect the results, as we have a large distance between the dots. We define the positions of the minima of the confinement potential as $(L_x,0)$, $(-L_x,0)$. Then the confinement potential can be written using x and y coordinates as

$$V_C(x,y)=\frac{1}{2}m^*\omega_0^2\times[x^2+y^2-2L_x|x|+L_x^2-2L_Tx]. \quad (5)$$

We use GaAs material parameters $m^*/m_e=0.067$ and $\epsilon=12.7$, and the confinement strength $\hbar\omega_0=3.0$ meV. This confinement corresponds to the harmonic oscillator length of $\sqrt{\hbar/\omega_0 m^*}\approx 20$ nm. External magnetic field is 200 mT.

The four-dimensional Schrödinger equation is discretized using a grid of around 20^4 points. We use finite difference method with five-point Laplacian. The eigenvalues and eigenvectors of the resulting Hermitian matrix are solved using the Lanczos diagonalization. The exchange energy J is simply obtained from the difference of the eigenenergies of the singlet and triplet states. The eigenenergies for the singlet and triplet states agree with the values obtained in a previous numerical study.[34]

Due to the hyperfine field, the wave function is not completely symmetric or antisymmetric. We obtain the spin expectation value from the wave function ψ by dividing it to a symmetric part ψ_S corresponding to the triplet state and antisymmetric part ψ_A corresponding to the singlet state

$$\psi(\mathbf{r}_1,\mathbf{r}_2)=\alpha\psi_S(\mathbf{r}_1,\mathbf{r}_2)+\beta\psi_A(\mathbf{r}_1,\mathbf{r}_2), \quad (6)$$

where $\alpha^2+\beta^2=1$ and α^2 is the singlet probability. When electrons are exchanged, we obtain

$$\psi(\mathbf{r}_2,\mathbf{r}_1)=\alpha\psi_S(\mathbf{r}_1,\mathbf{r}_2)-\beta\psi_A(\mathbf{r}_1,\mathbf{r}_2), \quad (7)$$

and this helps us to calculate P_S from integral,

$$\int\int d\mathbf{r}_1 d\mathbf{r}_2\psi^*(\mathbf{r}_1,\mathbf{r}_2)\psi(\mathbf{r}_2,\mathbf{r}_1)=2\alpha^2-1=2P_S-1. \quad (8)$$

We model the experimental control cycle used by Petta *et al.*,[13] where both electrons are initially in the right quantum dot, confined by the potential shown in the solid curve in Fig. 1. This state is called (0,2) below. Gradually the detuning parameter L_T is decreased so that a second potential minimum becomes degenerate with the first minimum, see dashed curve in Fig. 1. Now electrons are in both dots, in the state called (1,1).

In the (0,2) charge configuration, the triplet state has a much larger energy and it is energetically inaccessible, whereas in the (1,1) state both singlet and triplet states are accessible. As the electrons are in a random hyperfine field, the mean values of the hyperfine field in the left and right dot are slightly different, which causes the emergence of triplet states and singlet-triplet decoherence.

We calculate the time evolution of the wave function $\psi(\mathbf{r}_1,\mathbf{r}_2)$ when the potential is changed by the detuning parameter. The exponential of the Hamiltonian matrix is evaluated using a Krylov space method.[35] The randomness of the hyperfine field is taken into account by averaging the results over different hyperfine field realizations.

It turns out that using realistic parameters the separation of the quantum dots is an adiabatic process. The change in the detuning voltage is performed in 1 ns (Ref. 13), which is a short time compared to the decoherence timescale 10–1000 ns (Ref. 24). Thus the spin does not change significantly during the separation. We can model the spin evolution with a time-independent Hamiltonian. There is a large energy gap between the four lowest-lying states (S, T_0, and $T_{\pm 1}$) and higher excited states. Hence only the four lowest states are occupied and we may use perturbation theory for the evaluation of the effect of the hyperfine interaction. This method is much faster compared to the propagation of full exact diagonalization (ED) wave function. We begin the numerical simulation from the case of separated dots and solve for $\mathbf{B}_{\rm nuc}=0$ the singlet ground state and excited triplet state. These states are used for the calculation of the matrix elements of the hyperfine field. In the following, we denote $\mathbf{B}_l=g^*\mu_B\mathbf{B}_{\rm nuc}(\mathbf{r}_l)$, where $l=1,2$ and set $\hbar=1$. The perturbation term in the Hamiltonian due to the inhomogeneous hyperfine field is

$$H_{\rm hf}=\mathbf{B}_1\cdot\mathbf{S}_1+\mathbf{B}_2\cdot\mathbf{S}_2, \quad (9)$$

where $\mathbf{B}_l$ are the nuclear hyperfine fields and $\mathbf{S}_l=\frac{1}{2}(\sigma_{xl}+\sigma_{yl}+\sigma_{zl})$ are the spin operators for electrons $l=1,2$. The Hamiltonian is expressed in a scalar form as

$$H_{\rm hf}=\sum_{l=1}^{2}\frac{1}{2}(B_l^x\sigma_{xl}+B_l^y\sigma_{yl}+B_l^z\sigma_{zl}). \quad (10)$$

We calculate the elements of the Hamiltonian matrix in the basis of one singlet and three triplet states $\{|S\rangle,|T_1\rangle,|T_0\rangle,|T_{-1}\rangle\}$. The space parts of the wave functions of the triplet states are denoted with ψ_T and the singlet state correspondingly with ψ_S. We obtain the matrix elements from space integrals, e.g.,

$$\langle S|H_{\rm hf}|T_0\rangle=\frac{1}{2}\int\int d\mathbf{r}_1 d\mathbf{r}_2\psi_S^*(\mathbf{r}_1,\mathbf{r}_2)(B_1^z-B_2^z)\psi_T(\mathbf{r}_1,\mathbf{r}_2). \quad (11)$$

For the integral we use the shorthand notation,

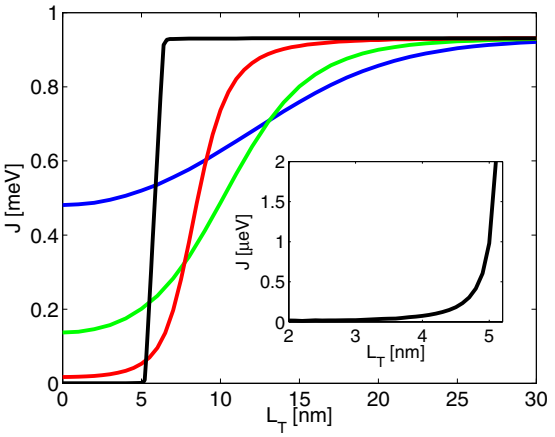

FIG. 2. (Color online) Exchange J as a function of detuning parameter L_T. From top to bottom at $L_T=0$ nm: $L_x=10$, 20, 30, and 50 nm. Distance between the dots is $d=2L_x$. Inset shows $L_x=50$ nm case zoomed in the region of small L_T values.

$$h_l^i = \int\int d\mathbf{r}_1 d\mathbf{r}_2 \psi_{S/T}^*(\mathbf{r}_1,\mathbf{r}_2) B_l^i \psi_{S/T}(\mathbf{r}_1,\mathbf{r}_2), \tag{12}$$

where the space parts of the wave functions $\psi_{S/T}^*, \psi_{S/T}$ are determined by the respective matrix element. In order to write the matrix elements compactly we use the variables[30]

$$h^i = \frac{1}{2}(h_1^i + h_2^i), \quad \delta h^i = \frac{1}{2}(h_1^i - h_2^i), \tag{13}$$

$$h^{\pm} = \delta h^x \pm i\delta h^y, \quad \delta h^{\pm} = h^x \pm i h^y, \tag{14}$$

and $\epsilon_Z = g^*\mu_B B^z$. We subtract the singlet energy from the diagonal matrix elements. The resulting Hamiltonian matrix H reads

$$\begin{pmatrix} 0 & -\delta h^+/\sqrt{2} & \delta h^z & \delta h^-/\sqrt{2} \\ -\delta h^-\sqrt{2} & J+\epsilon_Z+h^z & h^-/\sqrt{2} & 0 \\ \delta h^z & h^+/\sqrt{2} & J & h^-/\sqrt{2} \\ \delta h^+/\sqrt{2} & 0 & h^+/\sqrt{2} & J-\epsilon_Z-h^z \end{pmatrix},$$

corresponding to the result of Coish and Loss.[30] In our method all matrix elements are obtained from the ED calculation and the dots need not to be separate. The time evolution of the wave function $\psi(t)=[\alpha_1(t)\alpha_2(t)\alpha_3(t)\alpha_4(t)]^T$ is then simply obtained by $\psi(t)=\exp(-iHt)\psi(0)$.

III. RESULTS

The exchange energy J may be tuned by adjusting the detuning parameter L_T in the confinement potential V_c. Figure 2 presents the exchange energy J as a function of L_T for different interdot distances $d=2L_x$. We notice that the dependence of J on L_T approaches a step function with increasing L_x. Large L_T values correspond to a single parabolic quantum dot. Naturally, the exchange interaction diminishes with the growing distance of the dots. By a small detuning voltage, one can obtain large values of J even for large distances. The inset of Fig. 2 shows J for $2<L_T<5$ nm and $L_x=50$ nm. In this case changing L_T by 1 nm changes the voltage by 0.8 mV. The form of the curve is similar and the range in the values of L_T (3 nm, corresponding to 2.4 mV change in the voltage) correspond to the measurements of J for detuning voltage between 0 and 3 mV.[13] We use values shown in the inset for our simulations.

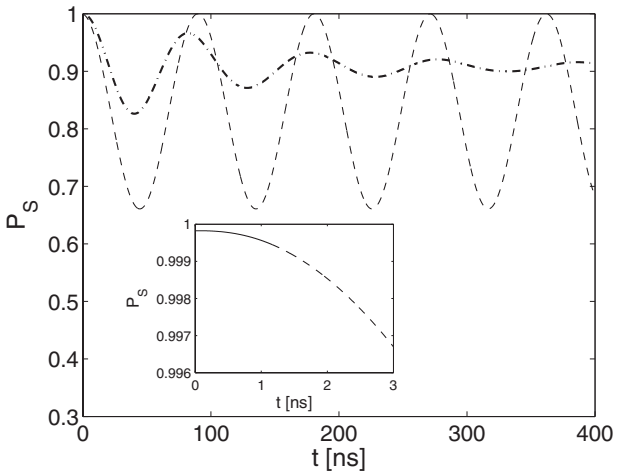

FIG. 3. Singlet probability P_S as a function of time t for $J=41$ neV and $L_x=50$ nm. Dashed line is a single realization and dash-dotted line is an average over 10^4 realizations. The inset is zoomed in the region of few nanoseconds and shows the singlet probability of a single realization obtained with full ED calculation (solid) until 1.2 ns and after that with the perturbation calculation (dashed).

Figure 3 shows the spin time evolution of a single hyperfine field realization for $J=41$ neV and $L_x=50$ nm. The inset shows spin evolution for the first few nanoseconds calculated from full exact diagonalization during the change of the detuning (up to 1.2 ns) and from perturbation theory after that. We notice that the change in spin from the beginning to 1.2 ns is small and the perturbation calculation continues smoothly the full ED calculation. As the calculation of time evolution of one nanosecond takes around 24 h of computer time, the evaluation of many realizations up to hundreds of nanoseconds is too time-consuming to do with full ED. In the case of one hyperfine field realization, the singlet probability P_S exhibits sinusoidal oscillation between one and a value between zero and one depending on the realization, see dashed curve in Fig. 3. However, when results are averaged over several hyperfine field realizations, the oscillation is damped and singlet probability saturates, see dash-dotted curve in Fig. 3.

In Fig. 4, we plot the numerical results for the singlet probability as a function of time for the $L_x=50$ nm case. The results are averaged over 10^4 nuclear configurations. We also show the experimental data of Laird *et al.* for comparison, extracted from Fig. 4 of Ref. 24. We use approximately the same values for J as found in the these experiments. The variance of the hyperfine field is difficult to determine in the calculation, because one unit cell given by the numerical grid contains of the order of thousands of GaAs atoms. Hence, the value of the hyperfine field in each grid point is an average of the hyperfine fields of the GaAs nuclei in the unit cell and as a result of this, the variance of the averaged hyperfine field

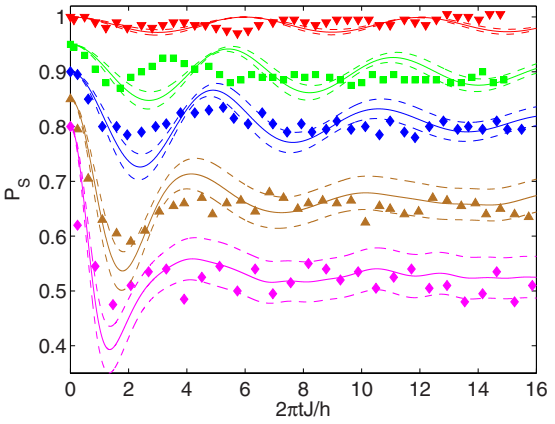

FIG. 4. (Color online) Measurements of Laird *et al.* (Ref. 24) with numerical results. From top to bottom: $J=133$ (red), 62 (green), 41 (blue), 22 (brown), and 12 neV (magenta). The unit time determined by J is from top to bottom, respectively, 5, 11, 16, 30, and 55 ns. The dashed lines give the standard error of the mean when the number of realizations is 50. The distance of the dots $2L_x$ is 100 nm. The curves are offset by 0.05 for clarity, i.e., all cases have $P_S=1$ at $t=0$.

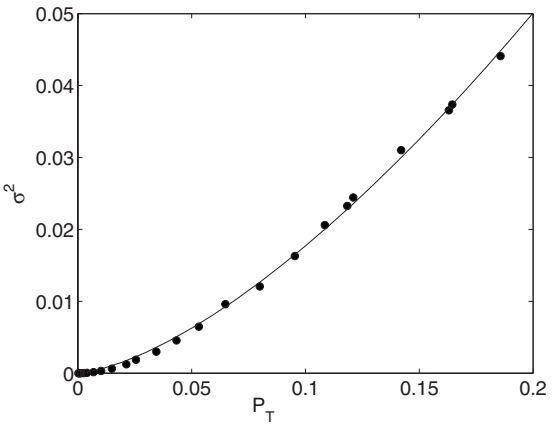

FIG. 5. Asymptotic triplet probability $\bar{P}_T$ and its variance σ^2. Solid line is a fit $\sigma^2=0.56(\bar{P}_T)^{1.5}$.

is reduced. We have fitted the variance of the hyperfine so that the asymptotic value of P_S for $J=62$ neV coincides with the experimental asymptotic value $P_S\approx 0.95$. This value of the variance has been used for other values of J and as Fig. 4 shows, the numerical saturation values of P_S match with the experimental findings for all other J values. In Ref. 24, the authors add an experimental visibility factor to explain their results using the model of Coish and Loss.[30] This is not used here, and we emphasize that we use only one experimental parameter when we fit the variance of the hyperfine field for $J=62$ neV.

Before we compare in detail our simulations with the experiments, it is useful to estimate the error bars. We calculate the standard deviation of the mean of $P_S(t)$ using 10^4 hyperfine field realizations. Then the standard error of the mean of $P_S(t)$ is estimated in the case of 50 realizations to mimic the experimental data. The error bars based on this estimate match with the deviation of the experimental results for large times. For small times, the simulations follow closely the experimental values. The initial descent of the curves is similar and the first minima for smaller values of J occur at the same time for simulations and experiments. For larger values of J, the numerical data has larger oscillations than that observed in the experiments. The oscillation in cases $J=62$ and 133 neV exhibits a phase difference between experimental and numerical values, but for smaller J the variance of the singlet probability is larger and the possible phase difference cannot be observed. This phase shift might not have a simple theoretical explanation, but it could be related to the tunneling coupling. Namely, in Fig. 4 of Ref. 24, there is a phase shift between the singlet probabilities for $J=131$ neV with small tunnel coupling and for $J=118$ neV with large tunnel coupling. This indicates that the tunnel coupling has an effect on the experimental results.

Figure 5 depicts the variance of the triplet probability $P_T=1-P_S$. The variance increases with the triplet probability, which was also evident in the experimental results,[24] where the fluctuation in the singlet probability values increases with a decreasing singlet probability. The values of the variance seem to depend on $P_T^{3/2}$, as the fit with the function $\sigma^2(P_T)=0.56(P_T)^{3/2}$ indicates.

It turns out in our perturbation calculation that the $|T_1\rangle$ and $|T_{-1}\rangle$ states have a vanishing occupancy, as expected when the external magnetic field exceeds the hyperfine field. In this case the perturbation is effectively described by the matrix,

$$H_{\text{eff}}=\begin{pmatrix} 0 & \delta h^z \\ \delta h^z & J \end{pmatrix}, \tag{15}$$

in the $|S\rangle-|T_0\rangle$ basis. Hence, the time evolution of the singlet probability depends solely on the ratio $\delta h^z/J$, as in the previous theoretical study.[30]

The exact time dependence of the singlet probability can now be calculated from the relation $\psi(t)=\exp(-iH_{\text{eff}}t)\psi(0)$. We denote $\psi(t)=[\alpha(t)\beta(t)]^T$ and use the initial condition $\psi(0)=(1\ \ 0)^T$. Then, using the exponential of 2×2 matrix, one can show that the singlet probability, given by $\alpha(t)^2$, is

$$P_S(t)=\frac{1}{2}\left[1+\frac{J^2}{D^2}+\left(1-\frac{J^2}{D^2}\right)\cos(Dt)\right], \tag{16}$$

where $D=\sqrt{4(\delta h^z)^2+J^2}$.

It is not trivial to average $P_S(t)$ over the hyperfine field distribution. However, this average turns out to be easy to calculate for the saturation value of P_S. This is based on the fact that the time average of the singlet probability $\bar{P}_S=\frac{1}{T}\int_0^T P_S(t)dt$ is equal to the asymptotic singlet probability $P_S(t=\infty)$ when the upper limit T of the time integral approaches infinity, as the initial oscillation does not affect the value of the integral. Using this, one finds the time average to be

$$\bar{P}_S=\frac{1}{2}\left(1+\frac{J^2}{D^2}\right). \tag{17}$$

Next, we average $\bar{P}_S$ over the hyperfine field realizations by integrating $\bar{P}_S$ over normally distributed values of the off-

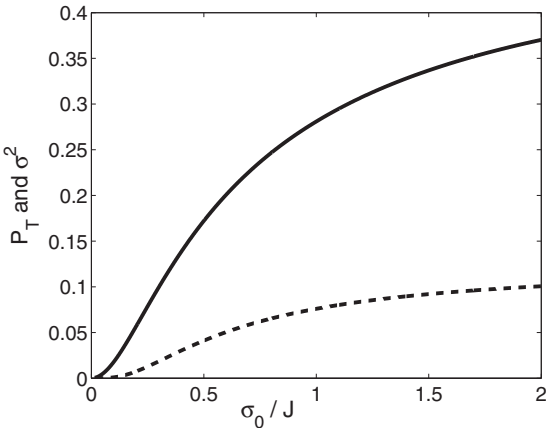

FIG. 6. Mean (solid) and variance (dashed) of the asymptotic triplet probability $1-\bar{P}_S$, calculated from Eqs. (19) and (20).

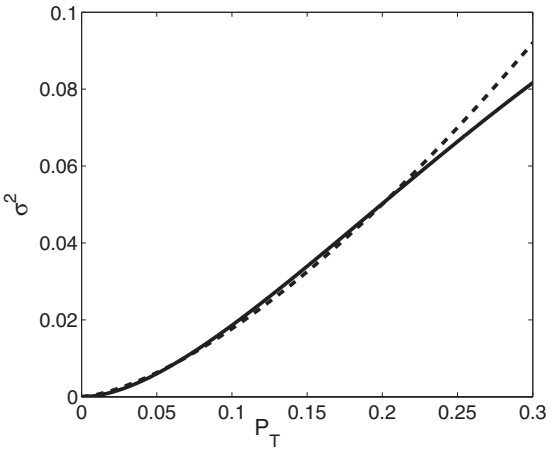

FIG. 7. The variance of the asymptotic triplet probability $\sigma^2(\bar{P}_T)$ as a function of $\bar{P}_T$. Dashed line is a fit $\sigma^2=0.56(\bar{P}_T)^{1.5}$.

diagonal matrix element δh^z. We assume δh^z distribution to have zero mean and variance σ_0^2. We use the notation $\delta h^z = x$ and obtain the average from

$$\langle \bar{P}_S \rangle = \frac{1}{2\sqrt{2\pi}\sigma_0} \int_{-\infty}^{\infty} \frac{\exp\left(-\frac{x^2}{2\sigma_0^2}\right)}{4\frac{x^2}{J^2}+1} dx + \frac{1}{2}, \tag{18}$$

which leads to the formula for the mean of the asymptotic singlet probability,

$$\langle \bar{P}_S \rangle = \frac{1}{2} + \sqrt{\frac{\pi}{2}} \frac{J}{4\sigma_0} \exp\left(\frac{J^2}{8\sigma_0^2}\right) \mathrm{erfc}\left(\frac{J}{2\sqrt{2}\sigma_0}\right). \tag{19}$$

We obtain in a similar fashion the variance of the asymptotic singlet probability $\sigma^2(\bar{P}_S)=\langle \bar{P}_S^2 \rangle - \langle \bar{P}_S \rangle^2$;

$$\sigma^2(\bar{P}_S) = \frac{J^3}{64\sigma_0^3}\left[-2\pi\frac{\sigma_0}{J}\exp\left(\frac{J^2}{4\sigma_0^2}\right)\mathrm{erfc}^2\left(\frac{J}{2\sqrt{2}\sigma_0}\right) - \left(\frac{\sigma_0^2}{J^2}+\frac{3}{4}\right)\sqrt{2\pi}\exp\left(\frac{J^2}{8\sigma_0^2}\right)\mathrm{erfc}\left(\frac{J}{2\sqrt{2}\sigma_0}\right) + \frac{\sigma_0}{J}\left(8\frac{\sigma_0^2}{J^2}+3\right)\right]. \tag{20}$$

The asymptotic triplet probability and its variance as a function of σ_0/J calculated using the formulas above are presented in Fig. 6. One can observe that the variance increases slowly and approaches 1/8 for $\sigma_0/J>1$. The triplet probability increases rapidly for $\sigma_0/J<1$, but then the curve starts to slope toward the limit $\bar{P}_T=1/2$. The variance of the triplet probability is shown in Fig. 7 as a function of the mean of the asymptotic triplet probability. This confirms our numerical results in Fig. 5 and the approximation $\sigma^2=0.56(\bar{P}_T)^{1.5}$ in the region $\bar{P}_T<0.2$. This approximation might serve as an additional calibration for the spin values and help to determine the visibility factor in the experiments.

IV. SUMMARY

In summary, we have studied the effect of exchange interaction on the singlet-triplet decoherence in a parabolic double quantum dot. We used exact diagonalization and perturbation theory for the calculation of the time evolution of the wave function. As a result, we observed damped oscillations and saturation values for the singlet probability. Our method allowed the evaluation of the exchange energy for different external voltages, which made possible a comparison to previous experimental data. The calculated singlet probabilities were in agreement with the results obtained in experiments.[13,24] The experimental saturation values corresponded very well to our numerical results. For larger values of the exchange energy, the phase of the spin oscillation differed from the experimental values. We estimated numerically the dependence of the variance of the asymptotic triplet probability $\sigma^2(\bar{P}_T)$ on the asymptotic triplet probability $\bar{P}_T$, which depends approximately on $\bar{P}_T^{3/2}$. We also derived expressions for the asymptotic singlet probability and its variance using a 2×2 effective Hamiltonian.

ACKNOWLEDGMENTS

This work was supported by the Academy of Finland through its Centers of Excellence Program (2006–2011). J.S. acknowledges financial support from the Magnus Ehrnrooth Foundation and the Finnish Cultural Foundation.

[1] D. Loss and D. P. DiVincenzo, Phys. Rev. A **57**, 120 (1998).
[2] G. Burkard, D. Loss, and D. P. DiVincenzo, Phys. Rev. B **59**, 2070 (1999).
[3] J. Levy, Phys. Rev. Lett. **89**, 147902 (2002).
[4] J. M. Taylor, H.-A. Engel, W. Dür, A. Yacoby, C. M. Marcus, P. Zoller, and M. D. Lukin, Nat. Phys. **1**, 177 (2005).
[5] R. Hanson and G. Burkard, Phys. Rev. Lett. **98**, 050502 (2007).
[6] R. Hanson, L. P. Kouwenhoven, J. R. Petta, S. Tarucha, and L. M. K. Vandersypen, Rev. Mod. Phys. **79**, 1217 (2007).
[7] F. H. L. Koppens, J. A. Folk, J. M. Elzerman, R. Hanson, L. H. Willems van Beveren, I. T. Vink, H. P. Tranitz, W. Wegscheider, L. P. Kouwenhoven, and L. M. K. Vandersypen, Science **309**, 1346 (2005).
[8] J. R. Petta, A. C. Johnson, A. Yacoby, C. M. Marcus, M. P. Hanson, and A. C. Gossard, Phys. Rev. B **72**, 161301(R) (2005).
[9] F. H. L. Koppens, C. Buizert, K. J. Tielrooij, I. T. Vink, K. C. Nowack, T. Meunier, L. P. Kouwenhoven, and L. M. K. Vandersypen, Nature (London) **442**, 766 (2006).
[10] T. Meunier, I. T. Vink, L. H. Willems van Beveren, K.-J. Tielrooij, R. Hanson, F. H. L. Koppens, H. P. Tranitz, W. Wegscheider, L. P. Kouwenhoven, and L. M. K. Vandersypen, Phys. Rev. Lett. **98**, 126601 (2007).
[11] A. C. Johnson, J. R. Petta, J. M. Taylor, A. Yacoby, M. D. Lukin, C. M. Marcus, M. P. Hanson, and A. C. Gossard, Nature (London) **435**, 925 (2005).
[12] K. Ono and S. Tarucha, Phys. Rev. Lett. **92**, 256803 (2004).
[13] J. R. Petta, A. C. Johnson, J. M. Taylor, E. A. Laird, A. Yacoby, M. D. Lukin, C. M. Marcus, M. P. Hanson, and A. C. Gossard, Science **309**, 2180 (2005).
[14] S. I. Erlingsson, Y. V. Nazarov, and V. I. Falko, Phys. Rev. B **64**, 195306 (2001).
[15] A. V. Khaetskii, D. Loss, and L. Glazman, Phys. Rev. Lett. **88**, 186802 (2002).
[16] A. V. Khaetskii, D. Loss, and L. Glazman, Phys. Rev. B **67**, 195329 (2003).
[17] I. A. Merkulov, A. L. Efros, and M. Rosen, Phys. Rev. B **65**, 205309 (2002).
[18] W. Zhang, V. V. Dobrovitski, K. A. Al-Hassanieh, E. Dagotto, and B. N. Harmon, Phys. Rev. B **74**, 205313 (2006).
[19] W. A. Coish and D. Loss, Phys. Rev. B **70**, 195340 (2004).
[20] A. V. Khaetskii and Y. V. Nazarov, Phys. Rev. B **61**, 12639 (2000).
[21] V. N. Golovach, A. Khaetskii, and D. Loss, Phys. Rev. Lett. **93**, 016601 (2004).
[22] J. M. Elzerman, R. Hanson, L. H. Willems van Beveren, B. Witkamp, L. M. K. Vandersypen, and L. P. Kouwenhoven, Nature (London) **430**, 431 (2004).
[23] S. Amasha, K. MacLean, Iuliana Radu, D. M. Zumbühl, M. A. Kastner, M. P. Hanson, and A. C. Gossard, arXiv:cond-mat/0607110 (unpublished).
[24] E. A. Laird, J. R. Petta, A. C. Johnson, C. M. Marcus, A. Yacoby, M. P. Hanson, and A. C. Gossard, Phys. Rev. Lett. **97**, 056801 (2006).
[25] R. G. Shulman, B. J. Wyluda, and H. J. Hrostowski, Phys. Rev. **109**, 808 (1958).
[26] D. Paget, Phys. Rev. B **25**, 4444 (1982).
[27] G. Giedke, J. M. Taylor, D. D'Alessandro, M. D. Lukin, and A. Imamoğlu, Phys. Rev. A **74**, 032316 (2006).
[28] D. Klauser, W. A. Coish, and D. Loss, Phys. Rev. B **73**, 205302 (2006).
[29] D. Stepanenko, G. Burkard, G. Giedke, and A. Imamoglu, Phys. Rev. Lett. **96**, 136401 (2006).
[30] W. A. Coish and D. Loss, Phys. Rev. B **72**, 125337 (2005).
[31] J. Schliemann, A. V. Khaetskii, and D. Loss, Phys. Rev. B **66**, 245303 (2002).
[32] N. Shenvi, R. de Sousa, and K. B. Whaley, Phys. Rev. B **71**, 224411 (2005).
[33] R. Nepstad, L. Sælen, and J. P. Hansen, Phys. Rev. B **77**, 125315 (2008).
[34] M. Helle, A. Harju, and R. M. Nieminen, Phys. Rev. B **72**, 205329 (2005).
[35] C. Moler and C. V. Loan, SIAM Rev. **45**, 3 (2003).